Constraints on the high-density nuclear equation of state from the phenomenology of compact stars and heavy-ion collisions

T. Klähn,[1,2,*] D. Blaschke,[3,4,†] S. Typel,[3] E. N. E. van Dalen,[2] A. Faessler,[2] C. Fuchs,[2] T. Gaitanos,[5] H. Grigorian,[1,6] A. Ho,[7] E. E. Kolomeitsev,[8] M. C. Miller,[9] G. Röpke,[1] J. Trümper,[10] D. N. Voskresensky,[3,11] F. Weber,[7] and H. H. Wolter[5]

[1]*Institut für Physik, Universität Rostock, D-18051 Rostock, Germany*
[2]*Institut für Theoretische Physik, Universität Tübingen, D-72076 Tübingen, Germany*
[3]*Gesellschaft für Schwerionenforschung mbH (GSI), D-64291 Darmstadt, Germany*
[4]*Bogoliubov Laboratory of Theoretical Physics, Joint Institute for Nuclear Research, Ru-141980 Dubna, Russia*
[5]*Department für Physik, Universität München, D-85748 Garching, Germany*
[6]*Department of Physics, Yerevan State University, 375049 Yerevan, Armenia*
[7]*Department of Physics, San Diego State University, 5500 Campanile Drive, San Diego, California 92182, USA*
[8]*School of Physics and Astronomy, University of Minnesota, Minneapolis, Minnesota 55455, USA*
[9]*Department of Astronomy, University of Maryland, College Park, Maryland 20742-2421, USA*
[10]*Max-Planck-Institut für extraterrestrische Physik, D-85741 Garching, Germany*
[11]*Moscow Engineering Physical Institute, Kashirskoe Shosse 31, Ru-11549 Moscow, Russia*

(Received 20 February 2006; published 21 September 2006)

A new scheme for testing nuclear matter equations of state (EoSs) at high densities using constraints from neutron star (NS) phenomenology and a flow data analysis of heavy-ion collisions is suggested. An acceptable EoS shall not allow the direct Urca process to occur in NSs with masses below $1.5M_{\odot}$, and also shall not contradict flow and kaon production data of heavy-ion collisions. Compact star constraints include the mass measurements of $2.1 \pm 0.2M_{\odot}$ (1σ level) for PSR J0751+1807 and of $2.0 \pm 0.1M_{\odot}$ from the innermost stable circular orbit for 4U 1636–536, the baryon mass—gravitational mass relationships from Pulsar B in J0737–3039 and the mass-radius relationships from quasiperiodic brightness oscillations in 4U 0614+09 and from the thermal emission of RX J1856–3754. This scheme is applied to a set of relativistic EoSs which are constrained otherwise from nuclear matter saturation properties. We demonstrate on the given examples that the test scheme due to the quality of the newly emerging astrophysical data leads to useful selection criteria for the high-density behavior of nuclear EoSs.

DOI: 10.1103/PhysRevC.74.035802 PACS number(s): 26.60.+c, 04.40.Dg, 12.38.Mh, 97.60.Jd

I. INTRODUCTION

The investigation of constraints for the high-density behavior of nuclear matter (NM) has recently received new impetus when the plans to construct a new accelerator facility (FAIR) at GSI Darmstadt were published. Among others a dedicated experiment for the investigation of the phase transition from hadronic matter to the quark-gluon plasma (QGP) in compressed baryon matter (CBM) shall be hosted, which will study the phenomena of chiral symmetry restoration and quark (gluon) deconfinement accompanying the transition to the QGP. A firm theoretical prediction for the critical baryon densities and temperatures of this transition in the QCD phase diagram as well as the existence and the position of a critical point depends sensitively on both the properties of NM at high densities and the model descriptions of quark-gluon matter in the nonperturbative regime close to the hadronization transition.

In the present work we apply recently discovered astrophysical bounds on the high-density behavior of NM in β- equilibrium, i.e., neutron star matter (NSM), from compact star cooling phenomenology and neutron star mass measurements together with information about the elliptical flow in heavy-ion collisions (HICs) in order to suggest a scheme for testing NM models. This new test scheme will be applied to candidates for the equation of state NM equation of state (EoS) which describe properties at the saturation density $n_s \approx 0.14$–$0.18\,\mathrm{fm}^{-3}$ such as the binding energy per particle in symmetric nuclear matter (SNM) a_v, the compressibility K and the asymmetry energy J and characteristics of large nuclei, such as the neutron skin, surface thickness and spin-orbit splitting probing the domain of subsaturation densities. In this paper we do not discuss the possibilities of various phase transitions, like hyperonization, pion and kaon condensations, quark matter, etc. [1–3]. Corresponding comments on how their inclusion could affect our results are added at the appropriate places.

While there are several NM models giving a rather similar description of the saturation and subsaturation behavior they differ considerably in their extrapolations to densities above $\sim 2n_s$, the regime which is relevant for NS physics and heavy-ion collisions. Recent progress in astrophysical observations and new insights into the compact star cooling phenomenology allow us to suggest in this paper a test scheme for the high density EoS which consists of five elements.

The first one demands that any reliable nuclear EoS should be able to reproduce the recently reported high pulsar mass of $2.1 \pm 0.2\mathrm{M}_{\odot}$ for PSR J0751+1807, a millisecond pulsar

*Electronic address: thomas.klaehn@uni-rostock.de
†Electronic address: blaschke@theory.gsi.de

in a binary system with a helium white dwarf secondary [4]. Extending this value even to 2σ confidence level ($^{+0.4}_{-0.5} M_\odot$) means that masses of at least $1.6 M_\odot$ have to be allowed. Thus the EoS should be rather stiff at high density to satisfy this constraint.

The second constraint has recently been suggested in Ref. [5] and concerns pulsar B in the double pulsar system J0737–3039 which has the lowest reliably measured mass for any NS to date, namely $M = 1.249 \pm 0.001 M_\odot$ [6]. If this star originates from the collapse of an ONeMg white dwarf [5] and the loss of matter during the formation of the NS is negligible, the baryon number, or equivalently the corresponding free baryon mass for the NS, has been determined to $1.366 M_\odot \leqslant M_N \leqslant 1.375 M_\odot$. It turns out that this constraint requires a rather strong binding of the compact star. A possible baryon loss of up to 1% of $M_\odot$ during the formation of the compact star broadens the corresponding baryon mass interval to $1.356 M_\odot \leqslant M_N \leqslant 1.375 M_\odot$.

The next constraint emerges from recent results of NS cooling calculations [7] and population synthesis models for young, nearby NSs [8]. Following the arguments in Refs. [7,9], direct Urca (DU) processes, e.g., the neutron β-decay $n \to p + e^- + \bar{\nu}_e$, produce neutrinos very efficiently. The neutrino emissivities for these processes even with inclusion of nucleon superfluidity effects are large enough that their occurrence would lead to an unacceptably fast cooling of NSs in disagreement with modern observational soft X-ray data in the temperature - age diagram. According to these recent analyses, the DU process shall not occur in typical NSs which have masses in the range of $M_{\rm typ} \sim 1.0$–$1.5 M_\odot$, obtained from population syntheses scenarios, since this would result in an overpopulation of X-ray dim isolated neutron stars in disagreement with the measured Log(N) - Log(S) distribution [8]. This constrains the density dependence of the nuclear asymmetry energy which should not be too strong.

The fourth constraint defines an upper bound in the mass-radius plane for NSs, derived from quasiperiodic oscillations (QPOs) at high frequencies of the low-mass X-ray binary (LMXB) 4U 0614+09 [10]. For some LMXBs there is evidence for the innermost stable circular orbit, which if confirmed suggests that the masses of the NSs in many of these systems are between 1.8 $M_\odot$ and 2.1 $M_\odot$ [11,12].

The fifth constraint comes from a recent analysis of the thermal radiation of the isolated pulsar RX J1856 which determines a lower bound for its mass-radius relation that implies a rather stiff EoS [13].

Finally, we include into the scheme constraints that are derived from analyses of elliptic flow data and from kaon production in heavy ion collisions. Nuclear collisions have been described within a kinetic theory approach and the results have been compared to experimental data for the nucleon flow for densities up to $4.5 \times n_s$ [14]. From this a region in the pressure-density diagram for SNM has been given which defines upper (UB) and lower (LB) bounds to the high density EoS and which is in accordance with measurements of the elliptic flow. Even though $4.5 \times n_s$ is below typical central densities that correspond to maximum masses of NS configurations we use the fact that the existence of such a region rules out rather stiff and very soft EoSs.

The outline of this work is the following. In Sec. II we describe a set of modern relativistic nuclear EoSs obtained within different approaches. In Sec. III the test scheme sketched above will be discussed in detail. This includes the astrophysical constraints from the determination of (maximum) NS masses in Sec. III A1, the new mass-baryon number test in Sec. III A2, constraints for DU-cooling in Sec. III A3 and for the mass-radius relations of LMXBs in Sec. III A4 as well as the mass-radius relation from thermal emission of the isolated NS RX J1856 in Sec. III A5. The EoS for SNM at supernuclear densities is constrained by HIC experiments from flow data analysis in Sec. III B1, and kaon production in Sec. III B2. In Section IV we derive two immediate consequences of this scheme: a conjecture about a universal symmetry energy contribution to the EoS in β-equilibrium and a sharpening of the flow constraint from HICs using new information about the masses of compact stars. A summary of the results of this work is given in Sec. V, together with the conclusions to be drawn from them.

II. HADRONIC EoS

A. Model independent description

There are numerous comparative studies of NM approaches for HIC and NS physics applications in which a representation of the NM EoS has been employed which is based on the nucleonic part of the binding energy per particle given in the form

$$E(n, \beta) = E_0(n) + \beta^2 E_S(n), \tag{1}$$

where $\beta = 1$–$2\,x$ is the asymmetry parameter depending on the proton fraction $x = n_p/n$ with the total baryon density $n = n_n + n_p$. In Eq. (1) the function $E_0(n)$ is the binding energy in SNM, and $E_S(n)$ is the (a)symmetry energy, i.e., the energy difference between pure neutron matter and SNM. Both contributions $E_0(n)$ and $E_S(n)$ are easily extracted from a given EoS for the cases $\beta = 0$ and $\beta = 1$, respectively. The parabolic interpolation has been widely used in the literature, see e.g., Ref. [15]. It proves to be an excellent parametrization of the asymmetry dependence for the purpose of the present study and we will not go beyond it here. Nevertheless, it should be mentioned in this context that an *exact reproduction* of a given EoS might require higher order terms than β^2 which have been neglected here. From Eq. (1) all zero temperature EoSs of NM can be obtained by applying simple thermodynamic identities [16]. In particular, we use the relations

$$\varepsilon_B(n, \beta) = nE(n, \beta), \tag{2}$$

$$P_B(n, \beta) = n^2 \frac{\partial}{\partial n} E(n, \beta), \tag{3}$$

$$\mu_{n,p}(n, \beta) = \left(1 + n\frac{\partial}{\partial n}\right) E_0(n) - \left(\beta^2 \mp 2\beta - \beta^2 n \frac{\partial}{\partial n}\right) E_S(n) \tag{4}$$

for the baryonic energy density $\varepsilon(n)$ and pressure $P(n)$ as well as the chemical potentials of neutron μ_n (upper sign) and proton μ_p (lower sign), respectively.

NSM has to fulfill the two essential conditions of β-equilibrium

$$\mu_n = \mu_p + \mu_e = \mu_p + \mu_\mu, \tag{5}$$

and charge neutrality

$$n_p - n_e - n_\mu = 0, \tag{6}$$

where μ_e and μ_μ are the electron and muon chemical potentials, conjugate to the corresponding densities n_e and n_μ. In this paper we do not consider phase transitions to a deconfined phase at $n > n_s$. If a first order phase transition were allowed a mixed phase could arise in some density interval, see Ref. [17]. In general, the local charge neutrality condition could be replaced by the global one. However, due to the charge screening this density interval is essentially narrowed [18,19].

Due to Eq. (5) the chemical potentials for muons and electrons are equal, $\mu_\mu = \mu_e$ so that muons appear in the system, once their chemical potential exceeds their mass. The EoS for NSM is considered as an ideal mixture of a baryonic and a leptonic part,

$$\varepsilon(n, \beta) = \varepsilon_B(n, \beta) + \varepsilon_e(n, \beta) + \varepsilon_\mu(n, \beta), \tag{7}$$

$$P(n, \beta) = P_B(n, \beta) + P_e(n, \beta) + P_\mu(n, \beta). \tag{8}$$

Under NS conditions one parameter is sufficient for a complete description, e.g., the baryochemical potential μ_b which is conjugate to the conserved baryonic charge. In β-equilibrated NSM and in SNM it is simply equivalent to the neutron chemical potential, $\mu_b = \mu_n$. Applying Eqs. (4) and (5) shows that the electron and muon chemical potential can be written as an explicit function of baryon density and asymmetry parameter,

$$\mu_e(n, \beta) = 4\beta E_S(n). \tag{9}$$

Both electrons and muons are described as a massive, relativistic ideal Fermi gas.

With the above relations only one degree of freedom, namely the baryon density, remains in charge neutral and β-equilibrated NSM at zero temperature. Within this comfortable description actual properties of NM depend on the behavior of $E_0(n)$ and $E_S(n)$ only. Both can be deduced easily from any EoS introduced in the following section.

B. Equations of state applied in this paper

A wide range of densities up to ten times the saturation density of NM is explored in the description of NSs and HICs. It is obvious that relativistic effects are important under these conditions. Consequently, we study only nuclear EoSs that originate from relativistic descriptions of NM. There are a number of different approaches from which we choose representative examples without attempting completeness. We want to emphasize that our focus is the development of a testing scheme rather than an exhaustive application of it.

Phenomenological models are based on a relativistic mean-field (RMF) description of NM with nucleons and mesons as degrees of freedom [20–23]. The mesons couple minimally to the nucleons. The coupling strengths are adjusted to properties of NM or atomic nuclei. A scalar meson (σ) and a vector meson (ω) are treated as classical fields generating scalar and vector interactions. The isovector contribution is generally represented by a vector meson ρ. In order to improve the description of experimental data, a medium dependence of the effective interaction has to be incorporated into the model. In many applications of the RMF model, nonlinear (NL) self-interactions of the σ meson were introduced with considerable success [24–33]. This approach was later extended to other meson fields [32]. As an alternative, RMF models with density-dependent nucleon-meson couplings were developed [33–38]. They allow for a more flexible description of the medium dependence and several parametrizations were introduced recently. In our study we choose two versions of the NL models with self-couplings of the σ meson field that were used in the simulation of HICs [39]. In the parameter set NLρ the isovector part of the interaction is described, as usual, only by a ρ meson. The set NL$\rho\delta$ also includes a scalar isovector meson δ that is usually neglected in RMF models [40]. It leads to an increased stiffness of the neutron matter EoS and the symmetry energy at high densities. These particular NL models were mainly constructed to explore qualitatively this scalar-isovector contribution in the symmetry energy. However, they have no non-linearity or density dependence in the isovector sector and lead to very, perhaps too, stiff symmetry energies at high densities. The density dependent RMF models are also represented here by two parameter sets [41]. They are obtained from a fit to properties of finite nuclei (binding energies, radii, surface thickenesses, neutron skins and spin-orbit splittings). The parametrization DD is the standard approach with constrained rational functions for the density dependence of the isoscalar meson couplings and an exponential function for the ρ meson coupling [35]. In the D^{3}C model additional couplings of the isoscalar mesons to derivatives of the nucleon field are introduced that lead to a momentum dependence of the nucleon self-energies that is absent in conventional RMF model [41].

Finally, we present a new parametrization of the RMF model with density-dependent couplings that is fitted to properties of finite nuclei (binding energies, charge and diffraction radii, surface thicknesses, neutron skin in ^{208}Pb, spin-orbit splittings) as in Ref. [41] with an additional flow constraint (see below) by fixing the pressure of SNM to $P = 50\,\mathrm{MeV\,fm^{-3}}$ at a density of $n = 0.48\,\mathrm{fm^{-3}}$. The density dependence of the σ and ω meson coupling functions is written as

$$\Gamma_i(n) = a_i \frac{1 + b_i(x + d_i)^2}{1 + c_i(x + d_i)^2} \Gamma_i(n_{\mathrm{ref}}), \tag{10}$$

where for the ρ meson a simple exponential law

$$\Gamma_\rho(n) = \Gamma_\rho(n_{\mathrm{ref}}) \exp[-a_\rho(x - 1)] \tag{11}$$

is assumed. The coupling constants $\Gamma_i(n_{\mathrm{ref}})$ have been fixed at a reference density n_{ref}. The density dependent couplings are functions of the ratio $x = n/n_{\mathrm{ref}}$ with the vector density n.

TABLE I. Parameters of the DD-F model as defined in Ref. [41] with a reference density of $n_{\rm ref} = 0.1469$ fm^3.

Meson i	m_i (MeV)	$\Gamma_i(n_{\rm ref})$	a_i	b_i	c_i	d_i
σ	555	11.024	1.4867	0.19560	0.42817	0.88233
ω	783	13.575	1.5449	0.18381	0.43969	0.87070
ρ	763	3.6450	0.44793			

The parameters of this parametrization called DD-F are specified in Table I. For a more detailed description of these type of models see Ref. [41].

More microscopic approaches start from a given free nucleon-nucleon interaction that is fitted to nucleon-nucleon scattering data and deuteron properties. In these *ab initio* calculations based on many-body techniques one derives the nuclear energy functional from first principles, i.e., treating short-range and many-body correlations explicitly. A successful approach to the nuclear many-body problem is the Brueckner hole-line expansion. In the relativistic Dirac-Brueckner-Hartree-Fock (DBHF) approach [42] the nucleon inside the medium is dressed by the self-energy Σ based on a T-matrix. The in-medium T-matrix which is obtained from the Bethe-Salpeter equation plays the role of an effective two-body interaction which contains all short-range and many-body correlations in the ladder approximation. Solving the Bethe-Salpeter equation the Pauli principle is respected and intermediate scattering states are projected out of the Fermi sea. The summation of the antisymmetrized T-matrix interactions with the occupied states inside the Fermi sphere yields finally the self-energy in Hartree-Fock approximation. This coupled set of equations constitutes a self-consistency problem which has to be solved by iteration. It is possible to extract the nucleon self-energies from DBHF calculations which can be compared with the corresponding quantities in phenomenological RMF models, but this is not completely unambiguous as discussed in Ref. [44]. Here, we use recent results of (asymmetric) NM calculations in the DBHF approach with the relativistic Bonn A potential in the subtracted T-matrix representation [43]. This calculation stands as a representative for a relativistic *ab initio* approach. One should, however, keep in mind that although state-of-the-art DBHF calculations [44–46] agree on a qualitative level, they show still some variance, depending on the choice of the interaction and the solution techniques applied. While implicitly included, present-day relativistic DBHF calculations do not include explicit three-body forces. They are essential in non-relativistic approaches such as BHF and variational calculations [47]. Due to the fact that three-body forces are to large extent unconstrained concerning their isospin dependence this introduces an additional source of uncertainty. For a detailed discussion of the various approaches see, e.g., Refs. [42,48].

In order to bridge the gap between fully microscopic and more phenomenological descriptions that can be applied more easily to various systems, it is often useful to adjust the parameters of the latter model to results extracted from the former method. As an example of this approach, we use a nonlinear RMF model (KVR) with couplings and meson masses depending on the σ-meson field [9]. The parameters were adjusted to describe the SNM and NSM EoS of the Urbana-Argonne group [47] at densities below four times the saturation density. Additionally, we study also a slightly modified parameter set (KVOR) of this RMF model that allows higher maximum NS masses. KVR and KVOR models elaborate the fact that not only the nucleon but also the meson masses should decrease with increasing NM density. Being motivated by the Brown-Rho scaling assumption, see Ref. [49], and the equivalence theorem between different RMF schemes, these models use only one extra parameter compared to the standard NL RMF model (NL model). The presence of this extra parameter allows one to eliminate a deficiency of conventional RMF models, consisting in a low critical density for the DU reaction.

The nuclear EoSs of these various models can be characterized by comparing the parameters in the approximation of the binding energy per nucleon

$$E = a_V + \frac{K}{18}\epsilon^2 - \frac{K'}{162}\epsilon^3 + \ldots + \beta^2\left(J + \frac{L}{3}\epsilon + \ldots\right) \quad (12)$$

around saturation as a function of the density deviation $\epsilon = (n - n_s)/n_s$ and the asymmetry β. In this form the EoS is characterized at saturation by the binding energy a_V, the incompressibility K and its derivative, the skewness parameter K' and by the symmetry energy J and the symmetry energy derivative or symmetry pressure L for asymmetric NM. In Table II these parameters are given for the models employed in this study. Additionally, we give the Dirac effective mass

TABLE II. Parameters of NM at saturation for various EoSs (see text).

Model	n_s (fm^{-3})	a_V (MeV)	K (MeV)	K' (MeV)	J (MeV)	L (MeV)	m_D (m)
NLρ	0.1459	−16.062	203.3	576.5	30.8	83.1	0.603
NL$\rho\delta$	0.1459	−16.062	203.3	576.5	31.0	92.3	0.603
DBHF	0.1810	−16.150	230.0	507.9	34.4	69.4	0.678
DD	0.1487	−16.021	240.0	−134.6	32.0	56.0	0.565
D^{3}C	0.1510	−15.981	232.5	−716.8	31.9	59.3	0.541
KVR	0.1600	−15.800	250.0	528.8	28.8	55.8	0.805
KVOR	0.1600	−16.000	275.0	422.8	32.9	73.6	0.800
DD-F	0.1469	−16.024	223.1	757.8	31.6	56.0	0.556

$m_D = m - \Sigma$ (at the Fermi momentum) in units of the free nucleon mass m depending on the scalar self-energy Σ of the nucleon.

There are significant differences between the models. The saturation density n_s in phenomenological models fitted to describe atomic nuclei (DD, D^{3}C, DD-F) is in the range 0.147–0.15 fm^{-3}. The models NLρ, NL$\rho\delta$ aiming at a description of low-energy HIC data use the still smaller value $n_s \simeq 0.146$ fm^{-3}. In contrast to that, the "*ab initio*" approach (DBHF) shows a saturation density that is considerably larger (0.181 fm^{-3}). Approximations of the Urbana-Argonne type EoS (KVR, KVOR) use 0.16 fm^{-3}. The binding energy per nucleon is very similar in all models. The incompressibility K spans a rather wide range from soft ($K \approx 200$ MeV) to rather stiff ($K \approx 275$ MeV). A major difference is found for the derivative K' of the incompressibility that is relevant for the densities above saturation. Models with parameters that are fitted to properties of finite nuclei (DD, D^{3}C) lead to a negative value of K' with a rather stiff EoS at higher densities. It is well known that the ratio of the surface tension to the surface thickness is determined by the parameters K and K' [50,51], however, the exact relation depends on the assumption for the shape of the surface. In the microscopic DBHF approach and the phenomenological models NLρ, NL$\rho\delta$, KVR, KVOR the parameter K' is rather large and, correspondingly, the EoS of symmetric matter is softer at high densities. The DD-F model constructed here is an exception. In this parametrization we wanted to satisfy simultaneously the description of finite nuclei and the flow constraint that requires a soft EoS at high densities leading to a very large K'. Correspondingly, the surface properties are not optimally well described by the DD-F model with clear systematic trends (radii too small for light nuclei and too large for heavy nuclei, too small surface thicknesses as compared to experimental data). We also remark that the parameters of the nonlinear models NLρ and NL$\rho\delta$, that where constructed for simulations of HICs, are not representative for conventional NL models that are fitted to properties of finite nuclei as, e.g., NL3, for which one finds $K = 271.5$ MeV, $K' = -203.0$ MeV, $J = 37.4$ MeV, $L = 100.9$ MeV and $m_D = 0.596\,m$ [31,41]. It is known that NL3 has an unphysically large symmetry energy. As was shown, e.g., in Ref. [52] this can be improved by inlcuding nonlinear rho-meson couplings. However, the resulting DU threshold mass and maximum NS mass proved to be rather small ($M_{\rm DU} = 1.3 M_\odot$ and $M_{\rm max} = 1.72 M_\odot$, see table 3 in Ref. [52]).

The symmetry energy J is very similar for all models with the exception of a slightly larger value in the DBHF calculation. Here one has, however, to keep in mind that this value is read off at a correspondingly larger density. At $n = 0.16\,\text{fm}^{-3}$ DBHF gives a value of $J = 31.5$ MeV, which is in good agreement with the empirical models and also with the variational approach of Ref. [47].

In contrast, the derivatives L of the symmetry energy of the various models are spread over a large range. This quantity is closely related to the stiffness of the symmetry energy at high densities. In order to describe the experimental neutron skin thicknesses in atomic nuclei a small slope of the neutron matter EoS is required [53–55]. Models with $L < 60$ MeV (DD, D^{3}C, KVR, DD-F) fulfill this requirement by introducing an effective density dependence of the ρ meson coupling to the nucleon which goes beyond conventional NL RMF models. A too small value for L on the other hand seems to be in conflict with data from isospin diffusion in heavy-ion collisions [56] so that recently from a combination of these data the limits 62 MeV $< L <$ 107 MeV have been suggested, see Ref. [57] and references therein. *Only the models NLρ, NL$\rho\delta$, DBHF, and KVOR satisfy this requirement*. However, as *our emphasis is on high density constraints of the EoS* we will not elaborate further on this interesting point here but remark that it deserves a proper treatment.

The Dirac effective mass m_D of the nucleon that appears in the relativistic dispersion relation of the nucleons also shows a large variation in the comparison. In order to describe the spin-orbit splitting in atomic nuclei, a small value, typically below or around $0.6m$ is required. Parameter sets with larger values (KVR, KVOR) might have a problem in this respect with the construction of a proper spin-orbit potential. Larger values of the effective Dirac nucleon mass are motivated by fitting the single nucleon spectra in nuclei [58] with a large Landau mass $m_L^* \simeq 0.9$–$1.0\,m$. The works [59] find $m_L^* \simeq 0.74$–$0.82\,m$ from the analysis of neutron scattering off lead nuclei. The latter values relate to $m_D \simeq 0.7$–$0.8\,m$ [1]. For a recent discussion of the momentum and isospin dependence of the in-medium nucleon mass, see, e.g., Ref. [44].

The variation in the NM parameters is directly reflected in the behavior of the energy per nucleon in SNM $E_0(n)$ and of the symmetry energy $E_S(n)$ at densities above saturation as shown in Fig. 1. The various models of this study predict considerably different values for $E_0(n)$ and $E_S(n)$ at high densities. Under the condition of β-equilibrium, however, the range of binding energy per nucleon $E(n, \beta)$ shows a much smaller variation than expected from $E_0(n)$ and $E_S(n)$. This is shown in the right panel of Fig. 1 and discussed further in Sec. IV.

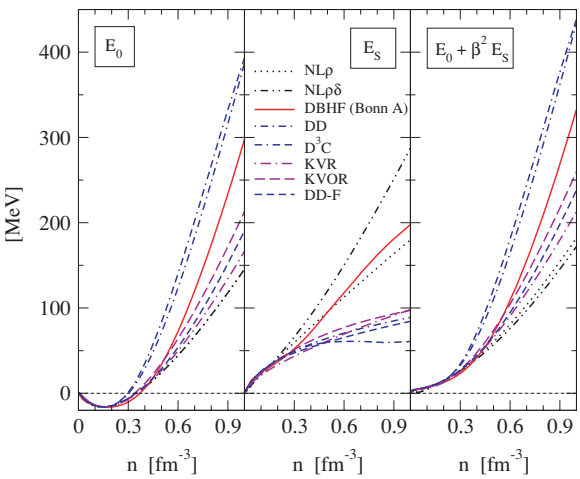

FIG. 1. (Color online) The energy per nucleon in SNM $E_0(n)$ (left panel), the symmetry energy $E_S(n)$ (middle panel) and the energy per nucleon in NSM (β-equilibrated and charge neutral) for the investigated models (right panel).

III. CONSTRAINTS ON THE EoS AT HIGH DENSITIES

In this section we will investigate to what extent the different EoSs introduced in Sec. II fulfill the various constraints. We postpone the discussion of the results of these tests to Sec. V after two new consequences from our analysis are presented in Sec. IV.

A. Constraints from compact stars

1. Maximum mass constraint

Measurements of "extreme" values, like large masses or radii, huge luminosities, etc., as provided by compact stars offer good opportunities to gain deeper insight into the physics of matter under extreme conditions as provided by compact stars. Recent measurements on PSR J0751+1807 imply a pulsar mass of $2.1 \pm 0.2(^{+0.4}_{-0.5})M_\odot$ (first error estimate with 1σ confidence, second in brackets with 2σ confidence) [4] which is remarkably heavy in comparison to common values for binary radio pulsars ($M_{\rm BRP} = 1.35 \pm 0.04 M_\odot$ [60]). This special result constrains NS masses to at least $1.6M_\odot$ (2σ confidence level) or even $1.9M_\odot$ within the 1σ confidence level.

The mass and structure of spherical, nonrotating stars, to which we limit ourselves in this paper, is calculated by solving the Tolman-Oppenheimer-Volkov (TOV) equation, which reads as

$$\frac{{\rm d}P(r)}{{\rm d}r} = -\frac{G[\varepsilon(r) + P(r)][m(r) + 4\pi r^3 P(r)]}{r[r - 2Gm(r)]}, \quad (13)$$

where the gravitational mass $m(r)$ inside a sphere of radius r is given by

$$m(r) = 4\pi \int_0^r {\rm d}r'\, r'^2 \varepsilon(r') \quad (14)$$

which includes the effects of the gravitational binding energy. The baryon number enclosed by that sphere is given by

$$N(r) = 4\pi \int_0^r \frac{{\rm d}r'\, r'^2 n(r')}{\sqrt{1 - \frac{2Gm(r')}{r'}}}, \quad (15)$$

with $n(r)$ being the baryon density profile of the star. Eq. (13) describes the gradient of the pressure P and implicitly the radial distribution of the energy density ε inside the star. In order to solve this set of differential equations, one has to specify the EoS, i.e., the relation between P and ε for which we take the EoSs introduced in the previous Sec. II. We supplement our EoSs describing the NSs interior by an EoS for the crust. For that we use a simple BPS model [61]. Due to uncertainties with different crust models one may obtain slightly different mass-radius relations.

The stellar radius R is defined by zero pressure at the stellar surface, $P(R) = 0$. The star's cumulative gravitational mass is given then by $M = m(R)$ and its total baryon number is $N = N(R)$. In order to solve the TOV equations the radial change of the pressure P starting with a given central value at radius $r = 0$ has to be calculated applying, e.g., an adaptive Runge-Kutta algorithm.

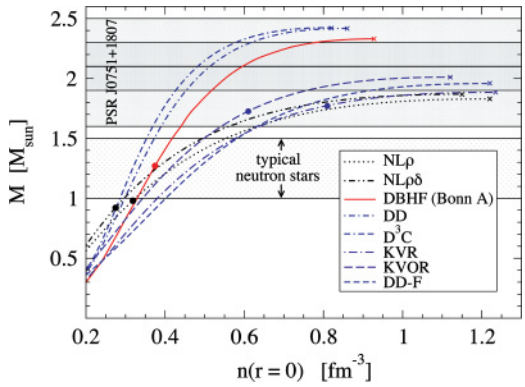

FIG. 2. (Color online) Mass versus central density for compact star configurations obtained by solving the TOV equations (13) and (14) for all EoSs introduced in Sec. III A Crosses denote the maximum mass configurations, filled dots mark the critical mass and central density values where the DU cooling process becomes possible. According to the DU constraint, it should not occur in "typical NSs" for which masses are expected from population synthesis [8] to lie in the lower grey horizontal band. The dark and light grey horizontal bands around $2.1M_\odot$ denote the 1σ and 2σ confidence levels, respectively, for the mass measurement of PSR J0751+1807 [4].

The resulting NS masses as a function of their central density for the different EoSs are given in Fig. 2 together with the mass range of typical NSs and the limits from PSR J0751+1807. Also shown in this figure are the points on the respective curves where the DU process becomes possible, as further discussed in Sec. III A3.

The maxima of the mass-central density relations are easily determined then and summarized in Table III for the EoSs investigated in this work. As can be seen none of these values falls below the 2σ mass limit of $1.6M_\odot$, whereas the 1σ mass limit of $1.9M_\odot$ would exclude NLρ and NL$\rho\delta$, while marginally excluding KVR. Thus the ability of this first and rather trivial test to exclude a given EoS demands a high accuracy of observations. A more stringent test could be achieved with decreasing error estimates or the observation of at least one pulsar that is still more massive than PSR J0751+1807. *We point out that if a pulsar with a mass $M > 2.1M_\odot$ is observed in the future, this will imply serious restrictions on the viable EoS*, see Fig. 2. Within the set of EoSs tested by us, only DD, D^{3}C, and DBHF would survive. Moreover, the maximum mass constraint is closely related to the flow constraint. This point will be further investigated within Sec. IV B.

2. Gravitational mass—baryon number constraint

Recently, it has been suggested in Ref. [5] that pulsar B in the double pulsar system J0737–3039 may serve to test models proposed for the EoS of superdense nuclear matter. The system J0737–3039 consists of a 22.7 ms pulsars J0737–3039A

TABLE III. Maximum star masses, corresponding central densities and the fulfillment of the strong (1σ) and weak (2σ) maximum mass constraint, as well as the gravitational mass-baryon number constraint for pulsar B in J0737–3039 [5] without and with a mass loss of $0.01M_\odot$. Fulfillment (violation) of a constraint is indicated with $+(-)$ and a marginal result is rated with $\circ$.

Model	$M_{\max}$ ($M_\odot$)	$n_{\max}(0)$ (fm^{-3})	J0751+1807 (1σ)	J0751+1807 (2σ)	J0737-3039 B (no loss)	J0737-3039 B (loss 1% $M_\odot$)
NLρ	1.83	1.22	−	+	−	−
NL$\rho\delta$	1.87	1.15	−	+	−	−
DBHF	2.33	0.94	+	+	−	+
DD	2.42	0.86	+	+	−	−
D^{3}C	2.42	0.82	+	+	−	−
KVR	1.89	1.24	$\circ$	+	−	+
KVOR	2.01	1.12	+	+	−	$\circ$
DD-F	1.96	1.22	+	+	−	+

(pulsar A) [62], and a 2.77 ms pulsar companion J0737–3039B (pulsar B) [63], orbiting the common center of mass in a slightly eccentric orbit of 2.4 h duration. One of the interesting characteristics of this system is that the mass of pulsar B is merely $1.249 \pm 0.001 M_\odot$ [6], which is the lowest reliably measured mass for any NS to date. Such a low mass could be an indication that pulsar B did not form in a type-II supernova, triggered by a collapsing iron core, but in a type-I supernova of an ONeMg white dwarf [5] driven hydrostatically unstable by electron captures onto Mg and Ne. The well-established critical density at which the collapse of such stars sets in is 4.5×10^9 g/cm^3 corresponding to an ONeMg core whose critical baryon mass is $M_N = Nu \sim 1.37 M_\odot$, where the atomic mass unit $u = 931.5$ MeV has been used [5] to convert the baryon number to baryon mass. Assuming that the loss of matter during the formation of the NS is negligible, a predicted baryon mass for the NS of $M_N = 1.366$–$1.375 M_\odot$ was derived in Ref. [5]. This theoretically inferred baryon number range together with the star's observed gravitational mass of $M = 1.249 \pm 0.001 M_\odot$ may represent a most valuable constraint on the EoS [5], provided the above key assumption for the formation mechanism of the pulsar B is correct. Then any viable EoS proposed for NSM must predict a baryon number in the range $1.366 \lesssim M_N \lesssim 1.375 M_\odot$ for a NS whose gravitational mass is in the range $M = 1.249 \pm 0.001 M_\odot$. *None of the EoSs tested in this work satisfies this strong constraint*. The authors of Ref. [5] discussed caveats such as baryon loss and variations of the critical mass due to carbon flashes during the collapse. This constraint requires a very precise calculation of the baryon number, e.g. a lowering of M_N by 1% changes the outcome of this test significantly. Since the simulation of e-capture supernovae and the evolution of their progenitors is still a work in progress, more interesting results are expected in the near future. The final value and accuracy of the baryon number of J0737–3039 are therefore highly important. The result of such calculations is shown in Fig. 3 and summarized in Table III. *Finally we point out that this constraint is critically based on the assumption of the formation scenario for pulsar B. If this turns out to be incorrect the constraint has to be abandoned.*

3. *Direct Urca constraint*

The maximum mass constraint seems to have, at least for the EoSs investigated in this paper, a rather small exclusion potential. The $M - M_N$ criterion, however, would provide more stringent limits only if the assumed formation mechanism of pulsar B in RX J0737–3039 and the neglect of mass loss prove to be valid. This scheme is improved by adding the DU criterion, which demands that the DU process shall not occur in typical neutron stars with masses in the range $M_{\rm typ} \sim 1$–$1.5 M_\odot$.

If the proton fraction $x = n_p/(n_p + n_n)$ exceeds a critical value $x_{\rm DU}$ the DU process $n \to p + e^- + \bar{\nu}_e$ becomes operative. An estimate of this DU-threshold follows from the triangle inequality for momentum conservation where the moduli of the momenta are given by the neutron, proton and electron

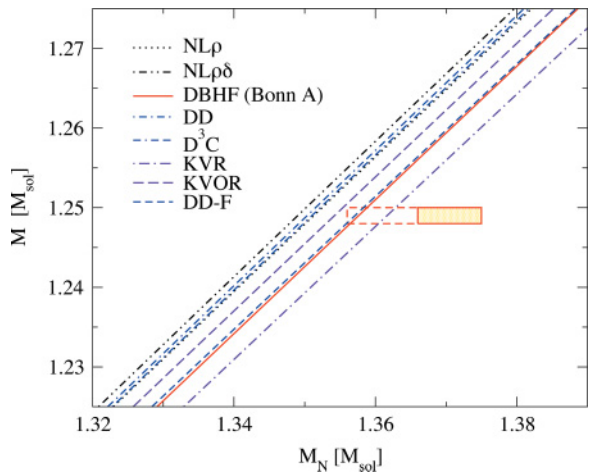

FIG. 3. (Color online) Relation between gravitational mass M and baryon mass M_N (both in units of the solar mass $M_\odot$) of NSs for the EoSs discussed in this work. The filled rectangle denotes the constraint derived for pulsar B in the double pulsar J0737–3039 [5]. The empty rectangle demonstrates the change of the constraint when the assumed loss of baryon number in the collapse amounts to 1% of the solar value.

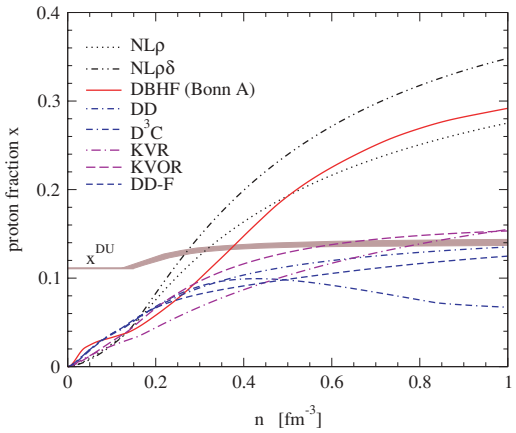

FIG. 4. (Color online) Proton fractions $x = n_p/(n_n + n_p)$ for different EoSs. The band labeled with $x_{\rm DU}$ frames all threshold curves obtained for the investigated models. According to Eq. (16) the range of possible threshold values varies between 11.1% and 14.8% depending on the muon fraction.

Fermi momenta p_{F_i}. The typical neutrino energy of the order of the temperature T is small and can be neglected. In quasi-equilibrium $n \to p + e^- + \bar{\nu}_e$ implies that $p_{F_n} \leqslant p_{F_p} + p_{F_e}$. From the charge neutrality condition $n_p = n_e + n_\mu$ one easily finds the DU-threshold $x_{\rm DU}$ as

$$x_{\rm DU} = \frac{1}{1 + \left(1 + x_e^{1/3}\right)^3}, \tag{16}$$

where $x_e = n_e/(n_e + n_\mu)$ is the leptonic electron fraction. Since this depends on the symmetry energy, the DU-threshold is model dependent. For $x_e = 1$ (no muons) this formula reproduces the muon-free threshold value of 11.1% [64]. In the limit of massless muons, which is applicable for high densities ($x_e = 1/2$) one finds an upper limit of $x_{\rm DU} = 14.8\%$. In Fig. 4 the proton fraction as a function of density is shown for the different EoSs, together with the slightly model-dependent DU-threshold $x_{\rm DU}(n)$, shown as a band for all the models. As can be seen the DU-process sets in at very different critical densities depending on the EoS. For some models (DD, D^3C, DD-F) the DU-process does not occur at all. Once the critical density is reached in the center of a star configuration for a given EoS, the corresponding DU-critical star mass $M_{\rm DU}$ is marked in Fig. 2 by a dot. Every star with a mass only slightly above $M_{\rm DU}$ will be efficiently cooled by the DU-process and becomes almost invisible for thermal detection within a few years [7]. Nucleon superfluidity which suppresses the cooling rates has been included. Values of the pairing gaps used in the literature have been used and then varied to check the model dependence of the result [65]. Table IV summarizes these DU critical masses for all models. The DU constraint is fulfilled by the DD, D^3C, and DD-F EoS models which are not affected by the DU process at all and by KVR, KVOR which are affected for masses higher than $1.5M_\odot$, the limit for "typical NS" obtained from population synthesis models [8,66]. As a weaker constraint we also use $M_{\rm DU} > 1.35M_\odot$, which follows from the population synthesis. If the DU process were allowed for $M_{\rm DU} < 1.35M_\odot$ it would affect most of the NS population and lead to a contradiction with the measured Log(N) - Log(S) distribution [8]. It should, however, not be expected that the objects observed in X-rays were some exotic family of NSs rather than typical NSs. DBHF and both NL models do not pass even the weak DU test. They have a DU threshold mass $M_{\rm DU} < 1.35M_\odot$. We remark that one can not, of course, finally exclude the possibility of lower values of $M_{\rm DU}$ within a more exotic explanation of the present cooling data. However, we consider the absence of the DU process for typical NS configurations as the most realistic scenario and define this as a constraint.

4. Mass-Radius relation constraint from LMXBs

The kilohertz quasi-periodic brightness oscillations (QPOs) seen from more than 25 NS X-ray binaries constrain candidate high-density EoSs because there are fundamental limits on how high-frequency such oscillations can be. A pair of such QPOs is often seen from these systems (see Ref. [67] for a general review of properties). In all currently viable models for these QPOs, the higher frequency of the QPOs is close to the orbital frequency at some special radius. For such a QPO to last the required many cycles (up to ∼100 in some sources), the orbit must obviously be outside the star. The orbit must also be outside the innermost stable circular orbit (ISCO), because according to the predictions of general

TABLE IV. Critical compact star mass for the occurrence of the DU cooling process with the corresponding central density, the criterion of the DU constraint and the M(R) constraints from the isolated NS RX J1856.5–3754 and the low-mass X-ray binary 4U 1636–536 with its upper (u) and lower (l) mass limits, see text. Symbols are defined in Table III.

Model	$M_{\rm DU}(M_\odot)$	$n_{\rm DU}(0)({\rm fm}^{-3})$	$M_{\rm DU} \geqslant 1.5M_\odot$	$M_{\rm DU} \geqslant 1.35M_\odot$	4U 1636-536 (u)	4U 1636-536 (l)	RX J1856 (A)	RX J1856 (B)	RX J1856 (C)
NLρ	0.98	0.32	−	−	−	−	−	−	+
NL$\rho\delta$	0.92	0.28	−	−	−	−	−	−	+
DBHF	1.27	0.37	−	−	+	+	−	+	+
DD	-	-	+	+	+	+	−	+	+
D^3C	-	-	+	+	+	+	−	+	+
KVR	1.77	0.81	+	+	−	○	−	−	+
KVOR	1.73	0.61	+	+	−	+	−	−	+
DD-F	-	-	+	+	−	+	−	−	+

relativity, inside the ISCO gas or particles would spiral rapidly into the star, preventing the production of sharp QPOs. This implies [10,68] that observation of a source whose maximum QPO frequency is $\nu_{\max}$ limits the stellar mass and radius to

$$M < 2.2\, M_\odot (1000\,\mathrm{Hz}/\nu_{\max})(1 + 0.75\, j)$$
$$R < 19.5\,\mathrm{km}(1000\,\mathrm{Hz}/\nu_{\max})(1 + 0.2\, j). \quad (17)$$

Here $j \equiv cJ/GM^2$ (where J is the stellar angular momentum) is the dimensionless spin parameter, which is typically 0.1–0.2 for these systems. There is also a limit on the radius for any given mass.

These limits imply that for any given source, the observed $\nu_{\max}$ means that the mass and radius must fall inside an allowed "wedge." Therefore, any allowed EoS must have some portion of its corresponding mass-radius curve fall inside this wedge. The wedge becomes smaller for higher $\nu_{\max}$, therefore the highest frequency ever observed (1330 Hz, for 4U 0614+091; see Ref. [69]) places the strongest of such constraints on the EoS. Note, though, that another NS could in principle have a greater mass and thus be outside this wedge, but an EoS ruled out by one star is ruled out for all, since all NS have the same EoS. As can be seen from Fig. 5, the current constraints from this argument do not rule out any of the EoS we consider. However, because higher frequencies imply smaller wedges, future observation of a QPO with a frequency ~1500–1600 Hz would rule out the stiffest of our EoS. This would therefore be a complementary restriction to those posed by RX J1856.5–3754 (discussed below) and the implied high masses for some specific NSs, which both argue against the softest EoS.

If one has evidence for a particular source that a given frequency is actually close to the orbital frequency at the ISCO, then the mass is known (modulo slight uncertainty about the spin parameter). This was first claimed for 4U 1820–30 [70],

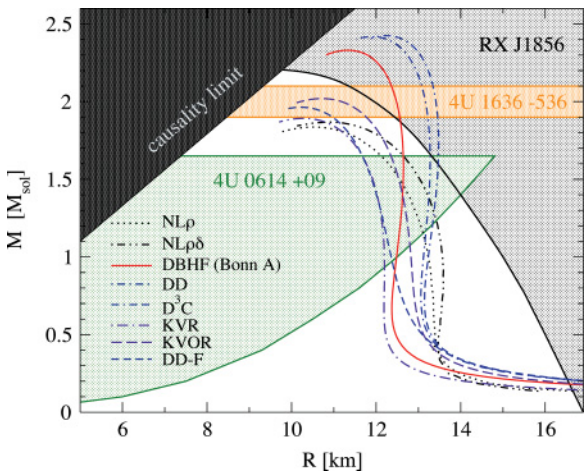

FIG. 5. (Color online) Mass-radius constraints from thermal radiation of the isolated NS RX J1856.5–3754 (grey hatched region) and from QPOs in the LMXBs 4U 0614+09 (green hatched area) and 4U 1636–536 (orange hatched region) which shall be regarded as separate conditions to the EoSs. For the mass of 4U 1636–536 a mass of $2.0 \pm 0.1 M_\odot$ is obtained, so that the weak QPO constraint would exclude the NLρ and NL$\rho\delta$ EoSs whereas the strong one would leave only DBHF, DD and D^{3}C.

but complexities in the source phenomenology have made this controversial. More recently, careful analysis of *Rossi* X-ray Timing Explorer data for 4U 1636–536 and other sources [11] has suggested that sharp and reproducible changes in QPO properties are related to the ISCO. If so, this implies that several NSs in low-mass X-ray binaries have gravitational masses between $1.9\, M_\odot$ and possibly $2.1\, M_\odot$ [11]. In Fig. 5 we display the estimated mass $2.0 \pm 0.1\, M_\odot$ for 4U 1636–536, which would eliminate NLρ and NL$\rho\delta$ as the softest proposed EoS even in the weak interpretation, and allow only DBHF, DD and D^{3}C in the strong one, see Table IV.

5. *Mass-Radius relation constraint from RX J1856*

The nearby isolated NS RX J1856.5–3754 (hereafter short: RX J1856) belongs to a group of seven objects which show a purely thermal spectrum in X-rays and in optical-UV. This allows the determination of R_∞/d, the ratio of the photospheric radius R_∞ to the distance d of the object, if the radiative properties of its photosphere are known. RX J1856 is the only object of this group which has a measured distance obtained by Hubble Space Telescope (HST) astrometry. Early measurements which turned out to be in error gave a distance of 60 pc and resulted in a very small blackbody radius of the neutron star which could not have been explained even in terms of a self-bound strange quark star [71]. After the corrected distance of 117 pc [72] became known several groups pointed out that the blackbody radius of this star is as large as 15–17 km. Although both the X-ray and the optical-UV spectra are extremely well represented by blackbody functions they require different emission areas, a smaller hot spot and a larger cooler region. The overall spectrum could also be fitted by blackbody emission from a surface showing a continuous temperature distribution between a hot pole and a cool equator as expected for a magnetized neutron star. The resulting blackbody radii are 17 (two blackbodies) and 16.8 km (continuous temperature distribution) [13]. In the present paper we use the result of the continuous temperature fit, $R_\infty = 16.8$ km. Recently, the inclusion of more HST sightings indicated even larger distances up to 178 pc, and 140 pc is considered to be a conservative lower limit [73]. This would yield unplausibly large radii, but recently it has been shown that a condensed matter surface radiating as a blackbody with a thin layer of magnetized hydrogen on top of it gives a very good fit to the overall spectrum. For a distance of 140 pc the corresponding radius is 17 km [74]. Although some questions, in particular that of the distance, are not yet finally settled, the recent data point to a large radius.

The relation between R_∞ and true stellar radius R is given by $R_\infty = R(1 - R/R_S)^{-1/2}$, with the Schwarzschild radius $R_S = 2GM/R$. It is also possible, that the surface could be condensed, in which case the inferences are less certain, but preliminary work [75] suggests that the radius is still likely to be large. The resulting lower bound in the mass radius plane for $R_\infty = 16.8$ km is shown in Fig. 5. There are three ways to interpret this result:

(i) RX J1856 belongs to compact stars with typical masses $M \sim 1.4 M_\odot$ and would thus have to have a radius

exceeding 14 km (see Fig. 2). *None of the examined EoSs can meet this requirement.*

(ii) RX J1856 has a typical radius of $R \sim 12$–13 km, implying that the EoS has to be rather stiff at high density in order to allow for configurations with masses above $\sim 2M_\odot$. In the present work this condition would be fulfilled for DBHF, DD and D^{3}C. This $M > 1.6M_\odot$ explanation implies that the object is very massive and it is not a typical NS since most of NSs have $M < 1.5M_\odot$, as follows from population synthesis models.

(iii) RX J1856 is an exotic object with a small mass $\sim 0.2M_\odot$, which would be possible for all EoSs considered here. *No such object has been observed yet*, but some mechanisms for their formation and properties have been discussed in the literature [76].

It cannot be excluded, however, that the distance measurement could be revised by a future analysis. If the distance would turn out to be smaller than the present value, then this constraint would have no discriminative power any more since all EoSs could possibly fulfill it. Should a revised distance value be larger than the present one, then only the exotic low-mass star interpretation would remain which again is possible for all (not self-bound) EoSs but which would raise the question about the formation scenario for such a diffuse low-mass object. Certainly this explanation of the puzzling object would no longer qualify RX J1856 as an object to test the high-density nuclear EoS.

Finally we want to emphasize another problem. Comparing Figs. 3 and 5 we observe that models producing a smaller radius (KVR, DD-F, DBHF) better accommodate the $M - M_N$ constraint and those having a larger radius (D^{3}C, DD) fulfill the RX J1856 constraints better. Out of the EoSs tested in this work only DBHF could satisfy these constraints simultaneously and it would be a rather challenging task to resolve the problem of this EoS with the DU constraint. Further comments are given in the discussion below.

B. Constraints from heavy-ion collisions

1. The flow constraint

The flow data analysis of dense SNM probed in HICs [14] reveals a correlation to the stiffness of the EoS which can be formulated as a constraint to be fulfilled within the testing scheme introduced here.

The flow of matter in HICs is directed both forward and perpendicular (transverse) to the beam axis. At high densities spectator nucleons may shield the transversal flow into their direction and generate an inhomogeneous density and thus a pressure profile in the transversal plane. This effect is commonly referred to as elliptic flow and depends directly on the given EoS. An analysis of these nucleon flow data, which depends essentially only on the isospin independent part of the EoS, was carried out in a particular model in Ref. [14]. In particular it was determined for which range of parameters of the EoS the model is still compatible with the flow data. The region thus determined is shown in Fig. 6 as the dark shaded region. Ref. [14] then asserts that this region limits the range of

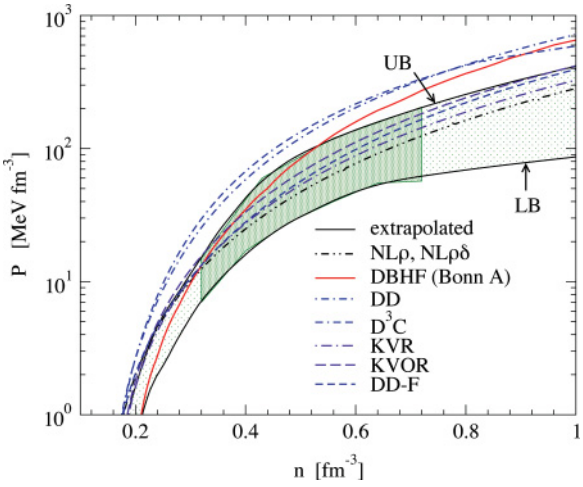

FIG. 6. (Color online) Pressure region consistent with experimental flow data in SNM (dark shaded region). The light shaded region extrapolates this region to higher densities within an upper (UB) and lower border (LB).

accessible pressure values at a given density. For our purposes we extrapolated this region by an upper (UB) and lower (LB) boundary, enclosing the light shade region in Fig. 6.

Thus the area of allowed values does not represent experimental values itself, but results from transport calculations for the motion of nucleons in a collision [14]. Of course, it seems preferable to repeat these calculations for each specific EoS, but this would not be a manageable testing tool. Therefore we adopt the results of Ref. [14] as a reasonable estimate of the preferable pressure-density domain in SNM. Its upper boundary is expected to be stable against temperature variations [77]. The important fact is that the flow constraint probes essentially only the symmetric part of the binding energy function $E_0(n)$.

Following Ref. [14] the constraint arises for a density window between 2 and 4.5 times saturation density n_s. One has, however, to keep in mind that at high densities this constraint is based on flow data from the AGS energy regime ($E_{\rm lab} \sim 4$–$11A$ GeV). At these energies a large amount of the initial bombarding energy is converted into new degrees of freedom, i.e., excitations of higher lying baryon resonances and mesons, which makes conclusions on the nuclear EoS more ambiguous than at low energies. Nevertheless, the analysis of Ref. [14] provides a guideline for the high density regime which we believe to be reasonable.

As can be seen in Fig. 6, this last constraint is well fulfilled by the KVR, KVOR, NLρ and NL$\rho\delta$ models. For the latter two models this is rather obvious since they have already been tested to reproduce flow data. The constraint is satisfied for densities below $3n_s$ by DBHF. When comparing our models with the flow constraint below, we separate regions of SIS ($n \lesssim 3n_s$) and AGS ($n \gtrsim\gtrsim 3n_s$) energies considering weak and strong flow constraints. DD and D^{3}C, which fulfilled the DU constraint well, are significantly above the demanded region. We want to emphasize that the DD-F model was constructed in this paper to pass this test. It is based on a reparametrization

of the DD model, in order to satisfy the introduced test scheme in most points.

2. *Constraints from subthreshold kaon production*

K^+ mesons were suggested as promising tools to probe the nuclear EoS, almost 20 years ago [78]. The first channel to open in order to produce a K^+ meson is the reaction $NN \longrightarrow N\Lambda K^+$ which has a threshold of $E_{\rm lab} = 1.58$ GeV kinetic energy for the incident nucleon. When the incident energy per nucleon in a heavy ion reaction is below this value one speaks of *subthreshold* kaon production. This process is particularly interesting since it ensures that the kaons originate from the high density phase of the reaction. The missing energy has to be provided either by the Fermi motion of the nucleons or by energy accumulating multi-step reactions. Both processes exclude significant distortions from surface effects if one goes sufficiently far below threshold. In combination with the long mean free path subthreshold K^+ production is an ideal tool to probe compressed NM in relativistic HICs, see Ref. [79] for a recent review.

Within the last decade the KaoS Collaboration at GSI has performed systematic measurements of the K^+ production far below threshold [80–82]. At subthreshold measurements which range from 0.6 to 1.5A GeV laboratory energy per nucleon compressions of two to maximally three times n_s are reached. Transport calculations have demonstrated that subthreshold K^+ production provides a suitable tool to constrain the EoS of SNM at supersaturation densities [79,83,84]. The theoretical analysis of the data implies a soft behavior of the EoS in the considered density range consistent with the flow constraint at moderate densities ($n \lesssim 3n_s$) and supports DBHF, NLρ, NL$\rho\delta$, KVR, KVOR and DD-F EoSs in SNM [85–87].

IV. CONSEQUENCES

A. Universal symmetry energy conjecture

Investigating the onset of DU processes in Sec. III A3 has shown that the DU threshold for the investigated models can be reached for rather small baryon densities slightly below $2n_s$ for NLρ, NL$\rho\delta$, DBHF or, as the most extreme opposite, not at all for DD, D^{3}C and DD-F. Equation (16) states that the threshold $x_{\rm DU}$ depends on the electron-muon ratio. The electron and muon densities are determined by their chemical potentials. In β-equilibrium $\mu_e = \mu_\mu$ is given in turn by Eq. (9) as a function of the asymmetry parameter β and the symmetry energy E_S. The resulting proton fraction x, shown on the right hand side of Fig. 7, mainly maps the topological behavior of $E_S(n)$, see Fig. 1. As a rule of thumb therefore a large proton fraction x is attained for stiff symmetry energies $E_S(n)$. The NLρ, NL$\rho\delta$ and DBHF models confirm this rule well and the symmetry energy used by these models can be sorted out for contradicting the present cooling phenomenology, as described in Sec. III A3. Figure 2 illustrates both DU- and maximum mass constraint.

The asymmetry contribution $\beta^2 E_S(n)$ to the energy per nucleon (left panel of Fig. 7) only shows a marginal dependence

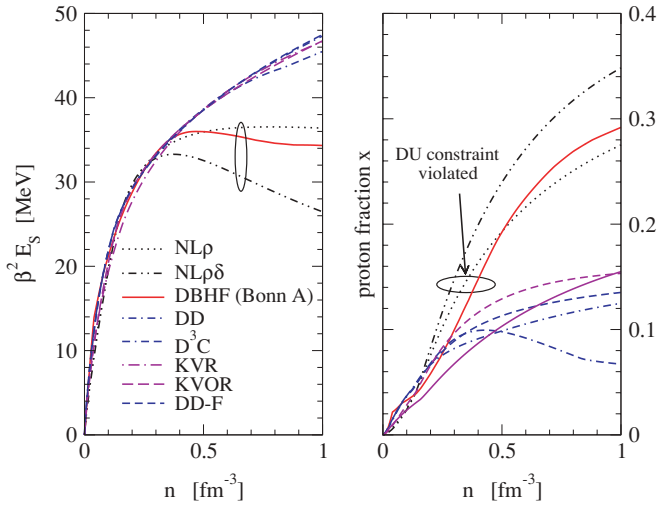

FIG. 7. (Color online) Density dependence of the asymmetry contribution to the energy per particle (left panel) and of the proton fraction (right panel) in NSM. Encircled curves correspond to EoSs that violate the DU-constraint.

for different EoSs when compared to differences in the energy per nucleon of SNM. These form a narrow band which allows two important statements. First, the behavior of $\beta^2 E_S(n)$ is to good approximation universal for all EoSs which pass the DU-constraint. The second conclusion regards the influence of the symmetry energy on the mass of NS. Here we find that due to the above universal behavior of $\beta^2 E_S(n)$ the mass of a star is also dominated by the behavior of $E_0(n)$. In other words it seems not very likely that it is possible to infer any essential properties of $E_S(n)$ only from NS mass observations, even if $E_0(n)$ would be perfectly known. This point emphasizes the importance of a more detailed understanding of the cooling behavior of compact stars as an effective tool for probing $E_S(n)$ at high densities beyond saturation.

B. Sharpening the flow constraint

As shown in Sec. III A1 and III B1 the flow constraint was more restrictive on the EoS than the maximum mass constraint due to a large estimated error for the mass of PSR J0751+1807. But the flow constraint itself has uncertainties, represented by the region of possible pressures in Fig. 6.

Thus an EoS which is in accordance with the flow constraint might still violate the maximum NS mass constraint. This is demonstrated in Fig. 8, where in particular the lower boundary of the limiting region in Fig. 6 was extrapolated to construct an artificial EoS (LB) in order to obtain the mass-density relation for corresponding compact star configurations.

The resulting mass curve in Fig. 8 is far from reaching even the weak mass constraint of $1.6M_\odot$ originating from the lower 2σ bound on the mass of PSR J0751+1807. It also cannot accommodate the well-measured mass $M_{B1913+16} = 1.4408 \pm 0.0003 M_\odot$ [88]. This figure clearly demonstrates that the lower bound (LB) in Fig. 6 does not satisfy the maximum mass constraint and should be shifted upwards, thus narrowing the band of the flow constraint.

TABLE V. Summary of results for the suggested scheme of tests. Non separated columns show the results for a strict (left) and weakened (right) interpretation of the corresponding constraint. The last column gives the total number of fulfilled tests in the suggested scheme. Symbols are defined in Table III.

Model	$M_{\max} \geqslant 1.9M_\odot$	$M_{\max} \geqslant 1.6M_\odot$	$M_{\rm DU} \geqslant 1.5M_\odot$	$M_{\rm DU} = \geqslant 1.35M_\odot$	4U 1636–536 (u)	4U 1636–536 (l)	RX J1856 (A)	RX J1856 (B)	J0737 (no loss)	J0737 (loss 1% $M_\odot$)	SIS+AGS flow constr.	SIS flow $+ K^+$ constr.	No. of passed tests	(out of 6)
NLρ	−	+	−	−	−	−	−	−	−	−	+	+	1	2
NL$\rho\delta$	−	+	−	−	−	−	−	−	−	−	+	+	1	2
DBHF	+	+	−	−	+	+	−	+	−	+	−	+	2	5
DD	+	+	+	+	+	+	−	+	−	−	−	−	3	4
D^3C	+	+	+	+	+	+	−	+	−	−	−	−	3	4
KVR	○	+	+	+	−	○	−	−	−	+	+	+	3	5
KVOR	+	+	+	+	−	+	−	−	−	○	+	+	3	5
DD-F	+	+	+	+	−	+	−	−	−	+	+	+	3	5

The maximum mass constraint demands a certain stiffness of $E_0(n)$ in order to obtain sufficiently large maximum NS masses. The small influence of $E_S(n)$ on the NS mass can be well recognized on Fig. 8, too. Two different symmetry energies, necessary to describe NSM, were taken from the investigated EoSs. They were chosen in accordance with the DU-constraint and gave the largest (DD-F) and smallest (D^3C) contribution to the binding energy at $n = 1\ \mathrm{fm}^{-3}$. The resulting deviations of the NS masses are shown as error bars on the curves in Fig. 8. It results in a maximum difference of less than $0.2M_\odot$ for the mass curves corresponding to LB. The same was done for an artificial EoS extrapolating the upper boundary (UB). Here the largest error estimate of approximately $0.1M_\odot$ is even smaller. The maximum mass for UB of about $2.0\,M_\odot$ again fulfills well the corresponding constraint.

Comparing the flow constraint in Fig. 6 and the mass-radius constraint in Fig. 5 we see that none of the EoSs we tested satisfies both constraints. Only DBHF is able to satisfy a weak flow constraint (for $n < 3n_s$) and the RX J1856 constraint under the assumption of an object with $M > 1.6M_\odot$. Thus we again emphasize a problem for the RX J1856 constraint with the joint fulfillment of other constraints as the $M - M_N$ and the flow constraints.

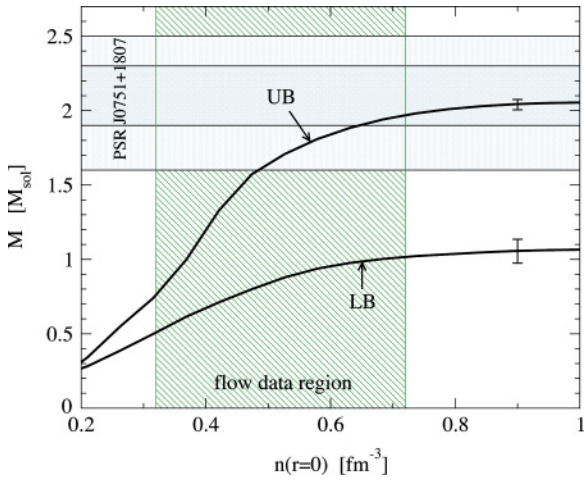

FIG. 8. (Color online) Mass versus central density for compact star configurations, calculated using the UB and LB extrapolations of the flow constraint boundaries from Fig. 6, $E_0(n)$, together with different symmetry energies $E_S(n)$ not violating the DU-constraint, see Fig. 7. The error bars illustrate the maximum deviation resulting from choosing different symmetry energies $E_S(n)$. The gray horizontal bars denote the expected mass of PSR J0751+1807 including for 1σ and 2σ confidence intervals, resp., whereas the vertical bars limit the density region covered by the flow constraint.

V. SUMMARY AND CONCLUSIONS

The task we intended with this work, developing a test scheme for the nuclear EoS by the present phenomenology of dense NM in compact stars and heavy-ion collisions, is satisfactorily completed at this point. Applying this scheme to specific EoSs offers some interesting insights which indicate that astrophysical measurements might become more important for the interpretation of terrestrial measurements than presently accepted. We have summarized the results of all suggested tests performed on our choice of relativistic, high-density EoSs in Table V which reveals the discriminative power of their combined application in a broad region of densities and isospin asymmetry. We want to point out here, however, that each model was derived to describe a restricted region in the (n, β)- plane and was not necessarily meant to describe a broader region. In Table V we rate the performance of the models when applied nevertheless in a very wide (n, β)-region.

Due to its sensitivity to different contributions to the energy this scheme motivates the necessity for changes in several EoSs if one wants to apply them to the whole available (n, β) interval although they well describe properties at the saturation density and a specific region of the (n, β) plane.

In particular $E_S(n)$, the contribution of the symmetry energy to the total energy, is probed by the DU-constraint. It states that the DU process would cool NSs much too fast, so that it should occur for stars with masses greater than ≈ 1.35–$1.5M_\odot$ only. If it would affect stars with masses below this limit the DU-process would affect most of the known NS population. We have shown that only EoSs with a rather soft symmetry energy at high density fulfill the DU-constraint.

The symmetric matter contribution to the energy per nucleon $E_0(n)$ should sufficiently describe the elliptic flow. Adding the results of Ref. [14] to the test scheme, very soft EoSs are allowed. The latter, however, can be sorted out by the maximum mass constraint. As a result, these two combined

constraints limit the stiffness of a reliable EoS to be rather low (flow), but not too low at $n \lesssim 4n_s$ and rather high for higher densities (maximum mass).

We want to stress that out of the tested EoSs only DBHF passes simultaneously the gravitational binding ($M - M_N$) as well as both mass-radius ($M - R$) tests. The $M - M_N$ constraint to be fulfilled requires a smaller radius of the $M \simeq 1.25 M_\odot$ star, whereas the $M - R$ test from RX J1856 favors substantially larger star radii, at least for $M \lesssim 1.4 M_\odot$. This contradictory situation would be resolved when RX J1856 is a star with a large mass or when an EoS would fulfill the $M - M_N$ constraint and nevertheless assign large radii to NS with typical masses. Such an EoS would be qualitatively different from the ones we investigate here.

The whole scheme left three of eight model EoSs, namely, DD-F, KVR, and KVOR as most effective within a broad (n, β) region under consideration. The DD-F model explicitly fits properties of finite nuclei, especially the neutron skin thickness of ^{208}Pb that implies a small value of L. The KVR model yields a similar value of L. It might, however, have problems with respect to isospin diffusion in heavy ion collisions since this small L does not fit the constraint deduced in Refs. [89] and [57]. The KVOR model fulfills this latter constraint. Here we point out that both KVR and KVOR were not applied to finite nuclei. Thus it would be a challenge to apply such models to finite nuclei in the future. All the models except DD-F demonstrate their predictive power within a broad (n, β) region whereas the DD-F model (as a modified DD model) has been constructed in the present work in order to fulfill the flow constraint in addition to constraints from saturation and finite nuclei common to DD models. In contrast to the phenomenological RMF models, DBHF is an ab initio approach without room left for the readjustment of free parameters. But correlations beyond the ladder approximation are not taken into account. In a certain sense, they are included, although hidden in the fitted parameters, in the phenomenological approaches. However, an interesting aspect would be to perform calculations for different types of free space nucleon-nucleon interactions. In particular the CD-Bonn potential [90] which accounts more precisely for the isospin dependence of the nuclear forces than Bonn A (used here) would be appropriate for future investigations. Another point would be the explicit inclusion of hyperonic degrees of freedom which may have a significant impact on the NS matter EoS at high densities (depending on yet badly known nucleon-hyperon interaction). This could open a possibility for the DBHF and other EoSs to satisfy appropriately the DU constraint.

Beside the scheme's good overall selectivity the joint application of different constraints might give new interesting insights. One of these is the universal behavior of the contribution $\beta^2 E_S(n)$ to the binding energy in NSM we observed for all EoSs that fulfill the DU-constraint. Then it seems to us that the flow constraint limits the maximum mass of NSs to values around or not much about the expected mass of PSR J0751+1807 with $M = 2.1 M_\odot$, which also coincides with the upper mass limit for 4U 1636–536. To verify this suggestion, a more detailed analysis, similar to that shown in Ref. [91], has to be performed.

Next we want to emphasize that the maximum mass constraint as a result of astrophysical measurements further limits the pressure-density-region which results from analysis of elliptic flow data governed in terrestrial HIC experiments [14]. Although the introduced scheme would not change, it seems useful to us to repeat these calculations under this point of view. It would be interesting too, to examine the agreement of experimental flow data with numerically calculated values explicitly applying the KVOR and DD-F models that have passed above constraints.

We have used here models which do not allow for phase transitions. Any possible phase transition that may appear in the NSs interior results in a decrease of the maximum NS mass. All the models may well pass the constraint $M_{\max} \lesssim 1.6 M_\odot$ (2σ uncertainty for PSR J0737–3039) but KVR, and even DD-F and KVOR which successfully have passed most of our tests might get problems with the restriction $M_{\max} \lesssim 1.9 M_\odot$ (1σ level for PSR J0737–3039 and lower limit for 4U 1636–536) if the phase transition is sufficiently strong.

If the phase transition would occur in SNM it would also soften the EoS thus modifying the flow constraint depicted in Fig. 4. Nevertheless, if the energy gain due to the phase transition is not too large the band of the flow constraint [14] is rather broad and all the models which already are situated within this band may still remain there. However, if we considered the common "flow+maximum mass" constraint as indicated by Fig. 6, the NLρ and NL$\rho\delta$ models could get a problem crossing the lower boundary of the thus obtained new band, again if the phase transition would be sufficiently strong.

The charged pion, kaon and the hyperonization transition in NSM change the proton and electron concentrations thus affecting the DU threshold. This threshold is then pushed up to higher densities. Simultaneously, these transitions open new reaction channels, allowing for DU reactions which involve new particles: π^-, K^-, hyperons and quarks. The appearance of the condensates and /or filling of the new Fermi seas also affects the values of the pairing gaps which are not well known. With small gaps the new reaction channels lead to very rapid cooling of NS raising the problem to appropriately describe the NS cooling. However, if gaps are large these reactions might be nonoperative and the DU constraint may become softer or even noneffective. The threshold densities for hyperonization strongly depend on poorly known baryon-baryon interactions. In case of repulsion the threshold density is pushed up [92] and the situation becomes more cumbersome. We avoided studying such models here.

We postpone the analysis of EoSs allowing for phase transitions to future work. Besides hyperonization, the possibility of a quark matter phase transition should be studied. This will be important for both NSs and for the planned HICs in the planned CBM experiment at FAIR where large baryon densities are to be created.

In this paper we presented a selection of constraints from compact star observables and HICs which focus on different aspects of the high density behavior of the EoS. Due to the increasing precision of present astrophysical measurements during the last years, which is expected to develop further, we feel confident that a stage is reached where the high

density EoS becomes testable by real constraints as we have demonstrated in this paper. However, the introduced scheme shall not be understood to be in a final shape, since the presented subtests will most likely sharpen with new arising data. Furthermore additional constraints might cover more aspects of the behavior of dense matter. We consider further investigations to be necessary as well as promising in order to work out deeper insights into the nature of dense matter beyond saturation, driven, e.g., by a systematic application of the presented scheme to more types of relativistic and nonrelativistic EoSs.

ACKNOWLEDGMENTS

The authors acknowledge discussions of the results presented in this work at the workshops on "The New Physics of Compact Stars" at the ECT* Trento, Italy, and on "Dense hadronic matter and QCD phase transition" in Prerow, Germany. T.K. has been supported in part by the DFG Graduate School 567 on "Strongly Correlated Many-particle Systems" at Rostock University and by the Virtual Institute VH-VI-041 on "Dense hadronic matter and QCD phase transition" of the Helmholtz Association. The work of D.N.V. has been supported in part by DFG project No. 436 RUS 113/558/0-3 and T.G. from the BMBF grant No. 06ML981. H.G. acknowledges funding from DFG grant No. 436 ARM 17/4/05, E.N.E.v.D. from grant FA 67/29-1. E.E.K. was supported by the U.S. Department of Energy under contract No. DE-FG02-87ER40328 and the research of F.W. is supported by the National Science Foundation (USA) under Grant PHY-0457329, and by the Research Corporation (USA). M.C.M. was supported in part by a senior NRC grant at Goddard Space Flight Center.

[1] N. K. Glendenning, *Compact stars: Nuclear physics, particle physics, and general relativity* (Springer, New York, 2000).
[2] F. Weber, *Pulsars as astrophysical laboratories for nuclear and particle physics* (IoP Publishing, London, 1999).
[3] *Superdense QCD matter and compact stars*, edited by D. Blaschke and D. Sedrakian (Springer, Dordrecht, 2006).
[4] D. J. Nice, E. M. Splaver, I. H. Stairs, O. Löhmer, A. Jessner, M. Kramer, and J. M. Cordes, Astrophys. J. **634**, 1242 (2005).
[5] P. Podsiadlowski, J. D. M. Dewi, P. Lesaffre, J. C. Miller, W. G. Newton, and J. R. Stone, Mon. Not. Roy. Astron. Soc. **361**, 1243 (2005).
[6] M. Kramer *et al.*, in *Proceedings of the 22nd Texas Symposium on Relativistic Astrophysics at Stanford, Stanford California, 2004*, edited by P. Chen *et al.*, Conf C041213, 0038 (2004).
[7] D. Blaschke, H. Grigorian, and D. Voskresensky, Astron. Astrophys. **424**, 979 (2004).
[8] S. Popov, H. Grigorian, R. Turolla, and D. Blaschke, Astron. Astrophys. **448**, 327 (2006).
[9] E. E. Kolomeitsev and D. N. Voskresensky, Nucl. Phys. **A759**, 373 (2005).
[10] M. C. Miller, AIP Conf. Proc. **714**, 365 (2004).
[11] D. Barret, J. F. Olive, and M. C. Miller, Mon. Not. Roy. Astron. Soc. **361**, 855 (2005).
[12] D. Barret, J. F. Olive, and M. C. Miller, arXiv:astro-ph/0510094.
[13] J. E. Trümper, V. Burwitz, F. Haberl, and V. E. Zavlin, Nucl. Phys. Proc. Suppl. **132**, 560 (2004).
[14] P. Danielewicz, R. Lacey, and W. G. Lynch, Science **298**, 1592 (2002).
[15] J. M. Lattimer and M. Prakash, Astrophys. J. **550**, 426 (2001).
[16] M. Baldo, G. F. Burgio, H. J. Schulze, Phys. Rev. C **61**, 055801 (2000).
[17] N. K. Glendenning, Phys. Rev. D **46**, 1274 (1992).
[18] D. N. Voskresensky, M. Yasuhira, and T. Tatsumi, Nucl. Phys. **A723**, 291 (2003).
[19] T. Maruyama, T. Tatsumi, D. N. Voskresensky, T. Tanigawa, and S. Chiba, Phys. Rev. C **72**, 015802 (2005).
[20] J. Walecka, Ann. Phys. (NY) **83**, 491 (1974).
[21] B. D. Serot and J. D. Walecka, Adv. Nucl. Phys. **16**, 1 (1986).
[22] P.-G. Reinhard, Rep. Prog. Phys. **52**, 439 (1989).
[23] P. Ring, Prog. Part. Nucl. Phys. **37**, 193 (1996).
[24] J. Boguta and A. R. Bodmer, Nucl. Phys. **A292**, 413 (1977).
[25] J. Boguta, Phys. Lett. **B106**, 250 (1981).
[26] P.-G. Reinhard, M. Rufa, J. Maruhn, W. Greiner, and J. Friedrich, Z. Phys. A **323**, 13 (1986).
[27] P.-G. Reinhard, Z. Phys. A **329**, 257 (1988).
[28] S. Gmuca, J. Phys. G **17**, 1115 (1991); Z. Phys. A **342**, 387 (1992); Nucl. Phys. **A547**, 447 (1992).
[29] M. M. Sharma, M. A. Nagarajan, and P. Ring, Phys. Lett. **B312**, 377 (1993).
[30] Y. Sugahara and H. Toki, Nucl. Phys. **A579**, 557 (1994).
[31] G. A. Lalazissis, J. König, and P. Ring, Phys. Rev. C **55**, 540 (1997).
[32] H. Toki *et al.*, J. Phys. G **24**, 1479 (1998).
[33] Wenhui Long, Jie Meng, Nguyen Van Giai, and Shan-Gui Zhou, Phys. Rev. C **69**, 034319 (2004).
[34] C. Fuchs, H. Lenske, and H. H. Wolter, Phys. Rev. C **52**, 3043 (1995).
[35] S. Typel and H. H. Wolter, Nucl. Phys. **A656**, 331 (1999).
[36] F. Hofmann, C. M. Keil, and H. Lenske, Phys. Rev. C **64**, 034314 (2001).
[37] T. Nikšić, D. Vretenar, P. Finelli, and P. Ring, Phys. Rev. C **66**, 024306 (2002).
[38] G. A. Lalazissis, T. Nikšić, D. Vretenar, and P. Ring, Phys. Rev. C **71**, 024312 (2005).
[39] T. Gaitanos, M. Di Toro, S. Typel, V. Baran, C. Fuchs, V. Greco, and H. H. Wolter, Nucl. Phys. **A732**, 24 (2004).
[40] B. Liu, V. Greco, V. Baran, M. Colonna, and M. Di Toro, Phys. Rev. C **65**, 045201 (2002).
[41] S. Typel, Phys. Rev. C **71**, 064301 (2005).
[42] C. Fuchs, Lect. Notes Phys. **641**, 119 (2004).
[43] E. N. E. van Dalen, C. Fuchs, and A. Faessler, Nucl. Phys. **A744**, 227 (2004); Phys. Rev. C **72**, 065803 (2005).
[44] E. N. E. van Dalen, C. Fuchs, and A. Faessler, Phys. Rev. Lett. **95**, 022302 (2005).
[45] T. Gross-Boelting, C. Fuchs, and A. Faessler, Nucl. Phys. **A648**, 105 (1999).

[46] F. de Jong and H. Lenske, Phys. Rev. C **58**, 890 (1998).
[47] A. Akmal, V. R. Pandharipande, and D. G. Ravenhall, Phys. Rev. C **58**, 1804 (1998).
[48] C. Fuchs and H. H. Wolter [nucl-th/0511070] Eur. Phys. J A (in press).
[49] G. E. Brown and M. Rho, Phys. Rev. Lett. **66**, 2720 (1991).
[50] W. Stocker, Phys. Lett. **B104**, 339 (1981).
[51] M. Farine, Z. Phys. A **331**, 375 (1988).
[52] B. G. Todd-Rutel and J. Piekarewicz, Phys. Rev. Lett. **95**, 122501 (2005).
[53] S. Typel and B. A. Brown, Phys. Rev. C **64**, 027302 (2001).
[54] R. J. Furnstahl, Nucl. Phys. **A706**, 85 (2002).
[55] L. W. Chen, C. M. Ko, and B. A. Li, Phys. Rev. C **72**, 064606 (2005).
[56] A. W. Steiner and B. A. Li, Phys. Rev. C **72**, 041601(R) (2005).
[57] B. A. Li and A. W. Steiner, arXiv:nucl-th/0511064.
[58] V. A. Khodel and E. E. Saperstein, Phys. Rep. **92**, 183 (1982).
[59] C. H. Johnson, D. J. Horen, and C. Mahaux, Phys. Rev. C **36**, 2252 (1987); C. Mahaux and R. Sartor, Nucl. Phys. **A475**, 247 (1987); M. Jaminon and C. Mahaux, Phys. Rev. C **40**, 354 (1989).
[60] S. E. Thorsett and D. Chakrabarty, Astrophys. J. **512**, 288 (1999).
[61] G. Baym, C. Pethick, P. Sutherland, Astrophys. J. **170**, 299 (1971).
[62] M. Burgay *et al*., Nature (London) **426**, 531 (2003).
[63] A. G. Lyne *et al*., Science **303**, 1153 (2004).
[64] J. M. Lattimer, C. J. Pethick, M. Prakash, and P. Haensel, Phys. Rev. Lett. **66**, 2701 (1991).
[65] H. Grigorian and D. N. Voskresensky, Astron. Astrophys. **444**, 913 (2005).
[66] S. E. Woosley, A. Heger, and T. A. Weaver, Rev. Mod. Phys. **74**, 1015 (2002).
[67] M. van der Klis, ARA&A **38**, 717 (2000).
[68] M. C. Miller, F. K. Lamb, and D. Psaltis, Astrophys. J. **508**, 791 (1998).
[69] S. van Straaten, E. C. Ford, M. van der Klis, M. Méndez, and P. Kaaret, Astrophys. J. **540**, 1049 (2000).
[70] W. Zhang, A. P. Smale, T. E. Strohmayer, and J. H. Swank, Astrophys. J. Lett. **500**, L171 (1998).
[71] J. A. Pons, F. M. Walter, J. M. Lattimer, M. Prakash, R. Neuhäuser, and P. An, Astrophys. J. **564**, 981 (2002).
[72] F. M. Walter and J. Lattimer, Astrophys. J. **576**, L145 (2002).
[73] D. Kaplan (private communication).
[74] W. Ho, in *Proceedings of the International Conference on Isolated Neutron Stars: From the Interior to the Surface, London, England, 24-28 April 2006*, Astrophys. Space Sci. (2006) to be published.
[75] W. Ho (private communication).
[76] S. B. Popov, arXiv:astro-ph/0403710.
[77] P. Danielewicz (private communication).
[78] J. Aichelin and C. M. Ko, Phys. Rev. Lett. **55**, 2661 (1985).
[79] C. Fuchs, Prog. Part. Nucl. Phys. **56**, 1 (2006).
[80] A. Schmah *et al*. (KaoS Collaboration), Phys. Rev. C **71**, 064907 (2005).
[81] C. Sturm *et al*. (KaoS Collaboration), Phys. Rev. Lett. **86**, 39 (2001).
[82] P. Senger and H. Ströbele, J. Phys. G **25**, R59 (1999).
[83] C. Fuchs, A. Faessler, E. Zabrodin, and Y. M. Zheng, Phys. Rev. Lett. **86**, 1974 (2001).
[84] C. Hartnack, H. Oeschler, and J. Aichelin, Phys. Rev. Lett. **96**, 012302 (2006).
[85] G. Stoicea *et al*. (FOPI Collaboration), Phys. Rev. Lett. **92**, 072303 (2004).
[86] A. Hombach, W. Cassing, S. Teis, and U. Mosel, Eur. Phys. J. A **5**, 157 (1999).
[87] T. Gaitanos, C. Fuchs, H. H. Wolter, and A. Faessler, Eur. Phys. J. A **12**, 421 (2001).
[88] I. H. Stairs, Science **304**, 547 (2004).
[89] L. W. Chen, C. M. Ko, and B. A. Li, Phys. Rev. C **72**, 064309 (2005).
[90] R. Machleidt, Phys. Rev. C **63**, 024001 (2001).
[91] V. Kalogera and G. Baym, Astrophys. J. **470**, L61 (1996).
[92] E. E. Kolomeitsev and D. N. Voskresensky, Phys. Rev. C **68**, 015803 (2003).